Acta Pharmaceutica Sinica B 2019;9(5):923–936

Chinese Pharmaceutical Association
Institute of Materia Medica, Chinese Academy of Medical Sciences

Acta Pharmaceutica Sinica B

www.elsevier.com/locate/apsb
www.sciencedirect.com

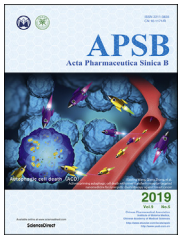

ORIGINAL ARTICLE

Inactivation of TFEB and NF-κB by marchantin M alleviates the chemotherapy-driven pro-tumorigenic senescent secretion

Huanmin Niu[a,†], Lilin Qian[a,†], Bin Sun[b], Wenjian Liu[a], Fang Wang[a], Qian Wang[a], Xiaotian Ji[a], Yanhai Luo[a], Effat Un Nesa[c], Hongxiang Lou[b], Huiqing Yuan[a,*]

[a]*Institute of Medical Sciences/Department of Biochemistry and Molecular Biology, the Second Hospital of Shandong University, Jinan 250033, China*
[b]*Key Laboratory of Natural Products & Chemical Biology, Ministry of Education, Department of Natural Products Chemistry, School of Pharmaceutical Sciences, Shandong University, Jinan 250012, China*
[c]*Department of Radiation Oncology, Qilu Hospital of Shandong University, Jinan 250012, China*

Received 1 July 2019; received in revised form 4 August 2019; accepted 19 August 2019

KEY WORDS

SASP;
Marchantin M;
TFEB;
NF-κB;
Drug resistance

Abstract It is critical to regulate the senescence-associated secretory phenotype (SASP) due to its effect on promoting malignant phenotypes and limiting the efficiency of cancer therapy. In this study, we demonstrated that marchantin M (Mar-M, a naturally occurring bisbibenzyl) suppressed pro-inflammatory SASP components which were elevated in chemotherapy-resistant cells. Mar-M treatment attenuated the pro-tumorigenic effects of SASP and enhanced survival in drug-resistant mouse models. No toxicity was detected on normal fibroblast cells or in animals following this treatment. Inactivation of transcription factor EB (TFEB) and nuclear factor-κB (NF-κB) by Mar-M significantly accounted for its suppression on the components of SASP. Furthermore, inhibition of SASP by Mar-M contributed to a synergistic effect during co-treatment with doxorubicin to lower toxicity and enhance antitumor efficacy. Thus, chemotherapy-driven pro-inflammatory activity, seen to contribute to drug-resistance, is an

Abbreviations: ALT, glutamic-pyruvic transaminase; AST, transaminase; BUN, blood urea nitrogen; CDDP, cisplatin; CM, conditioned media; CI, combinatory index; CREA, creatinine; CT-like, both chymotrypsin-like; DMSO, dimethyl sulfoxide; Doc, docetaxel; Doxo, doxorubicin; EdU, 5-ethynyl-2′-deoxyuridine; LPS, lipopolysaccharide; Mar-M, Marchantin M; MTT, 3-(4,5-dimethylthiazol-2-yl)-2,5-diphenyltetrazolium bromide; NF-κB, nuclear factor-κB; PGPH, peptidylglutamyl hydrolyzing; PI, propidium iodide; ROS, reactive oxygen species; SASP, senescence-associated secretory phenotype; SA-β-gal, senescence-associated β-galactosidase; Sv, starvation; TCGA, the Cancer Genome Atlas; TFEB, transcription factor EB; Tg, thapsigargin.

*Corresponding author.
E-mail address: lyuanhq@sdu.edu.cn (Huiqing Yuan).
[†]These authors made equal contributions to this work.

Peer review under responsibility of Institute of Materia Medica, Chinese Academy of Medical Sciences and Chinese Pharmaceutical Association.

https://doi.org/10.1016/j.apsb.2019.08.007

important target for Mar-M. By decreasing SASP, Mar-M may be a potential approach to overcome tumor malignancy.

1. Introduction

Although much improvement has been achieved in cancer therapy, cancer malignant progression is still a huge challenge, owing to cancer aggressiveness and drug-resistance. Although anti-cancer therapeutic agents are highly effective in killing cancer cells, these drugs also promote cellular senescence, a process which induces the loss of cellular proliferative capacity. Cellular senescence, resulting in irreversible cell cycle arrest can be triggered in many cell types (including cancer cells) in response to telomere-shortening, oncogene activation, chemotherapy, DNA damage, or oxidative stress[1−3]. Senescent cells undergo many phenotypic alterations, such as an enlarged and flattened morphology, metabolic reprogramming, autophagy modulation, upregulation of $P53/P21^{CIP1}$ and $P16^{INK4a}$/Rb, and senescence-associated β-galactosidase (SA-β-gal) activity[4]. Another important hallmark feature of senescence is the secretion of numerous inflammatory cytokines, growth factors and proteases, which is termed senescence-associated secretory phenotype (SASP)[5]. The SASP is physiologically beneficial for tissue repair and wound healing[6]. However, the secretion of inflammatory cytokines and matrix metalloproteinase in SASP influences neighboring cells and microenvironment by paracrine activities, resulting in acceleration of aging, as well as onset of the secondary cancers and some of the side effects of chemotherapy[7,8]. Given the fact that senescent cells act as a double-edged sword in human cancers, pro-senescent and anti-senescent therapies are actively being explored[9,10].

Cell-based screening of chemical libraries are potential strategies to discover new agents with limited adverse effects. Such strategies might induce cancer cellular senescence at low concentrations or mitigate the deleterious effects of senescent cells by either eliminating senescent cells and/or targeting the SASP. Some of these compounds naturally occurring in fruits, vegetables, tea, or wine that exhibit anti-senescent effects may also induce senescence in cancer cells[11,12]. For example, epigallocatechin-3-gallate and quercetin, two common polyphenols in tea, fruits and vegetables, are able to delay replicative senescence in chronically treated cells, and reduce expression of interleukin (IL)-6, IL-8 and IL-1β that are components of SASP in human foreskin fibroblasts during stress induced senescence[13,14]. Resveratrol protects human lung fibroblasts against high-glucose triggered oxidative stress and cellular senescence[15]. However, resveratrol also induced senescence in human lung cancer cells[16]. Similarly, doxorubicin (Doxo) and cisplatin (CDDP), two clinically used anti-cancer agents, are efficient in generating senescence in cell culture in addition to their effects on apoptosis activation[2]. Therefore, further research on the effect of bioactive compounds on senescence is necessary. We have investigated the novel macrocyclic bisbibenzyl-based class of agents that were isolated from liverwort plants, as bioactive compounds to exert antitumor and anti-inflammatory activities[17,18]. The present study went a further step to test the effect of marchantin M (Mar-M) on the SASP. Using multidrug resistant prostate cancer cells as a model (which are resistant to chemotherapy accompanied with high levels of pro-inflammatory factors), we discovered that Mar-M induced cellular senescence to suppress drug resistant cell growth without affecting normal fibroblast cells. Importantly, Mar-M reduced the secretion of SASP components by suppressing of their upstream regulator transcription factor EB (TFEB) and nuclear factor-κB (NF-κB), leading to the decreased pro-tumorigenic impact of SASP.

2. Materials and methods

2.1. Reagents

Marchantin M was isolated from Chinese *Liverworts*[17]. It was dissolved in dimethyl sulfoxide (DMSO) and stored at −20 °C. Lipopolysaccharide (LPS) was purchased from Sigma−Aldrich (St. Louis, MO, USA). Thapsigargin (Tg) was purchased from Selleck (Houston, TX, USA). Doxorubicin (Doxo) and docetaxel (Doc) were purchased from the Second Hospital of Shandong University (Jinan, China).

2.2. Cell culture and treatments

Prostate cancer (PCa) PC3 cells (the cell Bank of Chinese Academy of Sciences, Shanghai, China) and docetaxel-resistant PC3/Doc cells, as previously described, were cultured in F12K medium supplemented with 10% fetal bovine serum (Invitrogen, Carlsbad, CA, USA) and 100 U/mL penicillin and 100 g/mL streptomycin. Lung adenocarcinoma H460 and paclitaxel-resistant H460/Tax cells, murine PCa RM1 cells (the Cell Bank of Chinese Academy of Sciences, Shanghai, China) and RM1/Doc cells (docetaxel-resistant cell line derived from RM1) were cultured in RPMI-1640 medium supplemented with 10% fetal bovine serum and antibiotics (pennicillin and streptomycin). 293T cells were cultured in DMEM medium. All these cells were routinely cultured 5% CO_2 at 37 °C. After treatment with chemicals, cells were collected for Western blotting or other assays, and the conditioned media were harvested to determine cytokines. DMSO was used as the control vehicle. The experiments were performed in duplicate and repeated three times.

2.3. Senescence β-galactosidase (SA-β-gal) staining

After treatment with chemicals, the cells were stained with senescence β-galactosidase staining kit (Cell Signaling Technology, Boston, MA, USA). The cells were washed with PBS, and fixed for 10−15 min with 1 × fixative solution. After washing in phosphate buffered saline (PBS), the cells were incubated overnight at 37 °C in β-galactosidase staining solution, and subjected to check the cells under a microscope for the development of blue color, which represents senescence.

2.4. Cell cycle assay

After treatment of PC3/Doc cells with chemicals for 1 and 5 days, cells were detected using propidium iodide (PI, Beyotime, Shanghai, China) staining with flow cytometry (BD Biosciences, San Jose, CA, USA).

2.5. 5-Ethynyl-2′-deoxyuridine (EdU) incorporation assay

EdU cell proliferation kit was purchased from Millipore (Danvers, MA, USA). Pretreatment with Mar-M, the cells were incubated 16 h at 37 °C in complete media supplemented with 10 μmol/L EdU. After washing in PBS, the cells were fixed and permeabilized. Reaction cocktail and DAPI (Beyotime) were then added. The fluorescence change of cells was detected with flow cytometry or microscope.

2.6. Western blot analysis

After treatment with Mar-M as indicated, PC3/Doc cells were washed with ice-cold PBS, lysed in RIPA lysis buffer containing fresh protease and phosphates inhibitor mixture (50 mg/mL aprotinin, 0.5 mmol/L phenylmethanesulfonyl fluoride, 1 mmol/L sodium orthovanadate, 10 mmol/L sodium fluoride and 10 mmol/L β-glycerolphosphate). Cell lysates were then prepared for Western blotting. Protein concentrations were quantified by BCA protein assay (Beyotime). Western blotting was performed as described previously. The blots were incubated with primary antibodies against P16, P21, P27, cyclin A, cyclin B, TFEB, TFE3, P65, p-P65, γ-H2AX (Cell Signaling Technology) overnight at 4 °C respectively, prior to probed with appropriate peroxides-conjugated secondary antibodies. Glyceraldehyde-3-phosphate dehydrogenase (GAPDH, Santa Cruz Biotechnology, Santa Cruz, CA, USA) and Histone H3 (H3, Cell Signaling Technology) served as an internal control.

2.7. Cell viability assay

The 3-(4,5-dimethylthiazol-2-yl)-2,5-diphenyltetrazolium bromide (MTT, Beyotime) assay was used to test cell viability. Cells were grown in 96-well plates at a density of 2×10^3 cells/well. After 18 h, they were cultured with fresh or conditioned media. After 24 h pretreatment, cells were incubated with 100 μL MTT for 4 h. The formazan salt that formed was solubilized by adding 100 μL DMSO and its amount were determined by measuring optical density at 570 nm using a plate reader (Bio-Rad, Hercules, CA, USA).

2.8. Real-time quantitative PCR

Cells were seeded into 6-well plates and received treatments as indicated. Total RNAs was extracted using an RNAiso plus kit (TaKaRa, Japan). Complementary DNA was synthesized through reverse transcription using ReverTra Ace qPCR RT Kit (TOYOBO, Japan). Quantitative PCR analysis of cDNA was performed with SYBR Green reaction master mix on a real-time PCR system (Eppendorf International, Germany). Target mRNA levels were normalized to the level obtained for GAPDH. Changes in transcript level were calculated using $DD^{\triangle Ct}$ method. The primers used in this experiment were listed in Supporting Information Table S1.

2.9. RNA interference

PC3/Doc cells were transiently transfected with P21 siRNA (described previously), P27 siRNA (described previously) using lipofectamine 2000 (Invitrogen) according to the manufacturer's instructions. After transfected for 48 h, cells were exposed to Mar-M for additional 72 h. Cells were stained with senescence β-galactosidase staining kit.

2.10. Detection of intracellular ROS

PC3/Doc were treated with Mar-M for 24 h, and then incubated with DCFH-DA (Beyotime) for 30 min. After washed twice with PBS, the cells were detected with flow cytometry. The hydroperoxide was used as positive control.

2.11. Analysis of antitumor efficiency and toxicity of Mar-M in vivo

Male BALB/c-nude mice and C57BL/6 mice (6-week old) were obtained from Animal Center of China Academy of Medical Sciences (Beijing, China). Human PCa PC3 cells and murine PCa RM1 were injected into the right flanks of the mice and allowed to establish tumors. When the tumors reached ~5 mm^3, the mice were given docetaxel at 5 mg/kg by intraperitoneal injections every 2 days for 5 times. After stopped for one week, the mice were then given docetaxel for another 5 times. The tumor samples were disrupted with sterile blades to give a cell suspension with media. By cultivating and detecting, the resistant capability of PC3/Doc and RM1/Doc cells were confirmed by MTT. The resistant cells were then infected with luciferase virus (HANBI, Shanghai, China) to obtain PC3/Doc-Luc and RM1/Doc-Luc cells.

PC3/Doc-Luc cells were routinely injected into the left flank of the mice and allowed to develop tumors. After the tumors reached ~5 mm^3, animals were randomly assigned to different groups ($n = 6$) and treated with 16 mg/kg Mar-M [Mar-M(H) group], 8 mg/kg Mar-M [Mar-M(L) group], 4 mg/kg Doxo (Doxo group), or combination of 4 mg/kg Mar-M plus 2 mg/kg Doxo (Mar-M+Doxo group). The injections were performed every 2 days for 2 weeks. The tumor volume and animal weight were measured and recorded. Tumor sizes were visualized on an IVIS Imaging System (Caliper life Sciences, Alameda, CA, USA). Living Image 3.1.0 software (Caliper Life Science) was used to calculate the photometry of the tumor. The volume (mm^3) was calculated from Eq. (1):

$$\text{Volume} = 0.5 \times L \times W^2 \quad (1)$$

where L represents length and W represents width. All animal experiments were approved by Ethics Committee of Shandong University School of Medicine (Jinan, China).

2.12. Detection of effect of SASP induced by Mar-M on tumor growth in vivo

The RM1/Doc cells (1×10^5) in 0.1 mL of physiological saline were injected into the right flank of the mice and allowed to

establish RM1/Doc homograft. Tumor-bearing mice were randomly assigned to control and administration groups ($n = 13$ for each group). After 10-day treatment with either Mar-M or Doxo, the animals were randomly divided into two groups for different analysis. One group was designed to examine the paracrine effect of SASP, which were secreted from tumors pretreated with chemicals, the mice ($n = 6$) were randomly chosen to introduce RM1/Doc-luciferase (RM1/Doc-Luc) cells into the other side of individual mouse by subcutaneous injection. At the end of the experiment, the whole blood was collected from mice for cytokine analysis, and all tumors were resected for immunohistochemistry and SA-β-gal staining. The other mice ($n = 7$ for each group) were maintained for survival analysis.

2.13. Statistical analysis

Western blotting and fluorescent images were analyzed on Image Pro Plus (v6.0, Media Cybernetics, Carlsbad, CA, USA). The data are presented as the mean ± SD and analyzed with GraphPad Prism software (GraphPad, La Jolla, CA, USA). Student's *t*-test or one-way ANOVA analysis was used for comparison among different groups. Kaplan−Meier and Cox proportional hazards analyses were used for survival analysis. All the experiments have been repeated at least three times. Values of $P < 0.05$ was considered to be statistically significant, indicated as $^{*}P < 0.05$, $^{**}P < 0.01$, and $^{***}P < 0.001$ in the figures.

3. Results

3.1. Mar-M induces senescence in drug-resistant cells, but not in normal fibroblast cells

Screening assays have identified several candidate bisbibenzyls as potential anti-inflammatory and antitumor agents[17,18]. As shown in Fig. 1A, we initially confirmed an effect of Mar-M on IL-6 secretion in PCa multi-drug resistant PC3/Doc cells where pro-inflammatory factors including IL-6 were significantly increased[19]. To test a possible action of the bisbibenzyls on SASP, the senescence induction was examined in cells exposed to Mar-M. After treatment of cells with Mar-M (1 μmol/L) for 1 or 5 days, PC3/Doc cells became enlarged and flattened, and showed increased activity of SA-β-gal, while most of the parent PC3 cells were SA-β-gal negative and remained unchangeable in morphology (Fig. 1B). Doxo (0.3 μmol/L) was included as a positive control to display senescence induction[1]. Cell viability measurements indicated that resistant PC3/Doc cells were more sensitive to Mar-M, but not to Doc and Doxo, as compared with the paired PC3 cells (Supporting Information Figs. S1A and B). Senescence-associated parameters were also observed in other drug-resistant cells, such as murine PCa RM1 and drug-resistant RM1/Doc cells (induced from C57BL/6 murine prostate tumor), lung cancer H460/Tax cells (taxol-induced), esophageal cancer EC109/CDDP cells (cisplatin-induced) (Supporting Information Fig. S1C). EdU incorporation assays showed that Mar-M significantly suppressed cell proliferation in PC3/Doc cells (Fig. 1C). The cell cycle analysis indicated that Mar-M caused accumulation of cells in the S phase (Fig. 1D), accompanied by reduced cyclin A and cyclin B (Fig. 1E). The time-dependent induction of $P21^{CIP1}$ and $P27^{KIP}$, cell cycle inhibitors associated with senescence, was also evident in Mar-M-treated cells, whereas $P16^{INK4a}$ almost remained unchanged (Fig. 1E). Also, Mar-M did not affect Rb activity (phosphor-Rb) and Rb expression (total Rb) (Fig. S1D). Therefore, the P16INK4a/Rb signal might not be critical in Mar-M-induced senescence. The $P21^{CIP1}$ induction was P53-independent because PC3 cells are P53 null. Knockdown of $P21^{CIP1}$, but not $P27^{KIP}$, noticeably alleviated senescence induced by Mar-M, as evidenced by the reduction of positive SA-β-gal cells (Fig. 1F), indicating that accumulation of $P21^{CIP1}$ was required for inhibition of cell proliferation and senescence in response to Mar-M.

Whether Mar-M has a similar effect on non-neoplastic cells was next determined, including non-neoplastic prostate epithelial cells (RWPE1) and human normal fibroblast cells (NHF). The results in Fig. 1G indicated that, in contrast to Doxo, Mar-M had little effect on senescence induction in RWPE1 cells. More importantly, Mar-M (concentrations range from 0.6 μmol/L to 20 μmol/L) had no inhibition on NHF cell proliferation. In fact this treatment to some extent, increased cell proliferation as evidenced by cell viability and EdU incorporation (Fig. 1H−J). Thus, Mar-M selectively induced drug-resistant cellular senescence that was largely dependent on $P21^{CIP1}$ regardless of P53 status, yet produced a protective effect against the development of senescence in normal cells.

3.2. Mar-M-mediated proteasome inhibition is important for senescence induction

Since Mar-M arrested cells in S phase, and activation of the DNA damage is a major mechanism that elicits senescence[4,8], we analyzed the changes in phosphorylated histone variant H2AX (γ-H2AX), a mark of DNA damage. As shown in Fig. 2A, an increased γ-H2AX was noted in cells after 1-day treatment with Mar-M, with significant enhancement following 5 days exposure. However, we did not observe changes in reactive oxygen species (ROS) after treatment with Mar-M (Fig. 2B), though oxidative stress is the main cause to induce senescence in response to chemicals[12]. To gain insight into potential mechanisms required for regulation of Mar-M induced senescence, proteasome activity was measured to determine the involvement in Mar-M-induced senescence. This was investigated because Mar-M was shown to exert antitumor activity by inhibition of proteasome activity[17]. As shown in Fig. 2C, both chymotrypsin-like (CT-like) and peptidylglutamyl hydrolyzing (PGPH) activities were significantly decreased in a time-dependent manner upon Mar-M treatment, while trypsin-like activity remained unchanged. MG132, an inhibitor of proteasome, served as a positive control. To validate the role of the proteasome activity in Mar-M induced senescence, ectopic expression of $\beta5$ and $\beta7$, two major subunits of proteasome, resulted in enhanced proteasome activity, and restored CT-like and PGPH activity that was decreased by Mar-M (Fig. 2D). The enhancement of proteasome activity was associated with increased cell proliferation in response to Mar-M (Fig. 2E and F). Also, induction of γ-H2AX by Mar-M was decreased in cells expressing of $\beta5$ and $\beta7$ when compared to the Mar-M treatment alone (Fig. 2G and H), which was associated with reversal of the senescence phenotype induced by Mar-M (Fig. 2I). These data indicated that senescence induction by Mar-M was ascribed to, at least in part, proteasome inhibition.

3.3. Mar-M suppressed senescent cells expressing SASP

To determine whether Mar-M influenced the secretion of SASP factors due to its anti-inflammatory effect, we first measured the

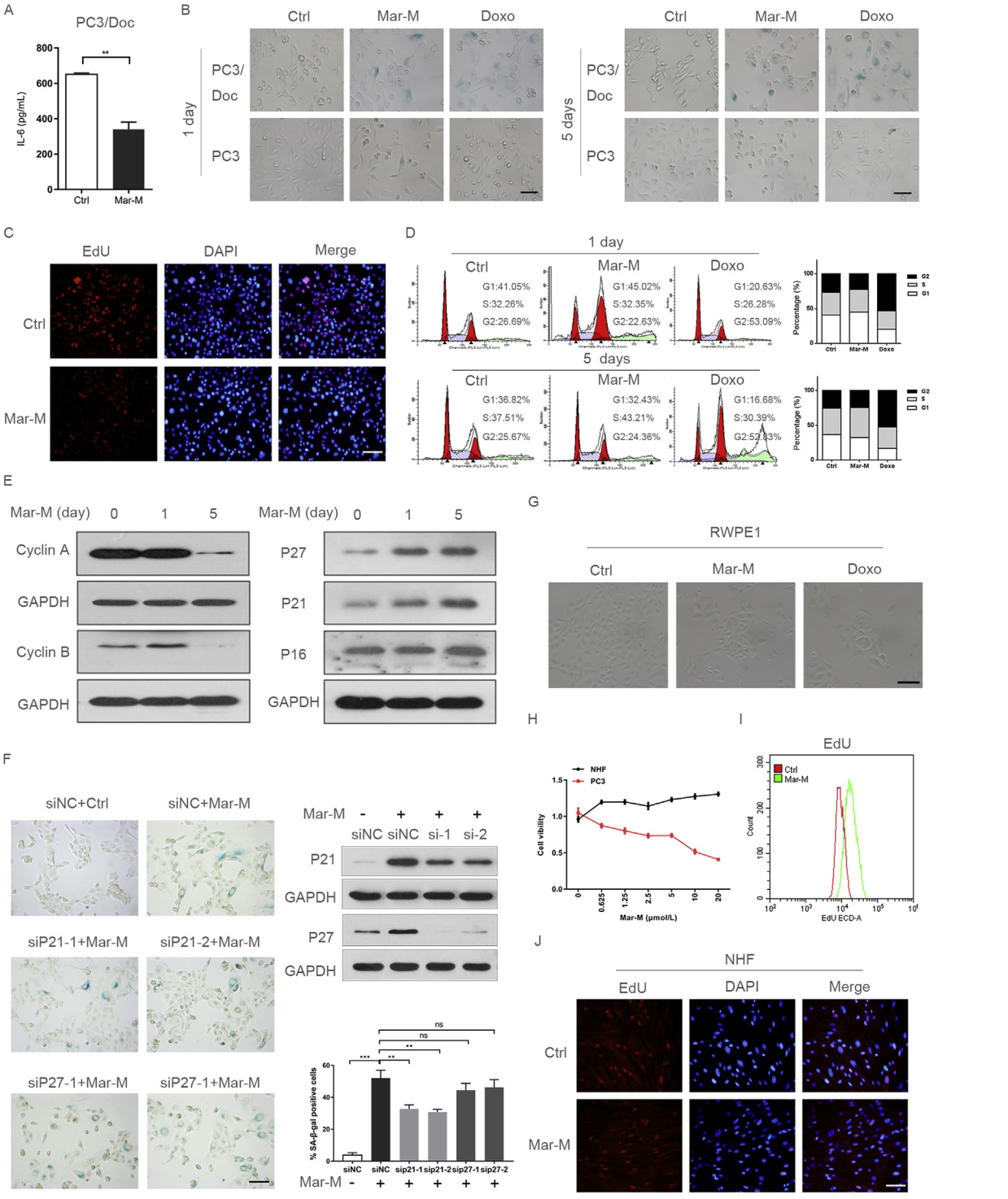

Figure 1 Mar-M induces senescence in drug resistant cells, but not in normal fibroblast cells. (A) The protein level of IL-6 in the cell culture supernatant measured using ELISA in PC3/Doc cells treatment with marchantin M (Mar-M) or doxorubicin (Doxo). (B) Detection of SA-β-gal activity in PC3/Doc cells and PC3 cells treated with Mar-M or Doxo for 1 and 5 days. (C) Proliferation of PC3/Doc cells treated with Mar-M was detected using EdU and stained with DAPI (to visualize nuclei). (D) PC3/Doc cells treated with Mar-M or Doxo for 1 and 5 days. Cell cycle analyses were performed by flow cytometry. (E) Western blot to detect the level of cell cycle proteins treated with Mar-M in PC3/Doc cells. (F) siRNA knockdown of P21 and P27 was performed in combination with Mar-M treatment and analysed the SA-β-gal activity. Bar graphs show SA-β-gal positive cells. (G) Detection of SA-β-gal activity in RWPE1 cells treated with Mar-M or Doxo for 5 days. (H) Survival rate of PC3, NHF treated with Mar-M. (I) EdU incorporation was monitored by flow cytometry in NHF cells treatment with Mar-M. (J) Representative fluorescent images of EdU staining in NHF cells. Results are representative of three independent experiments. Data are mean ± SD, $^{*}P < 0.05$, $^{**}P < 0.01$ and $^{***}P < 0.001$. Scale bar: 100 μm.

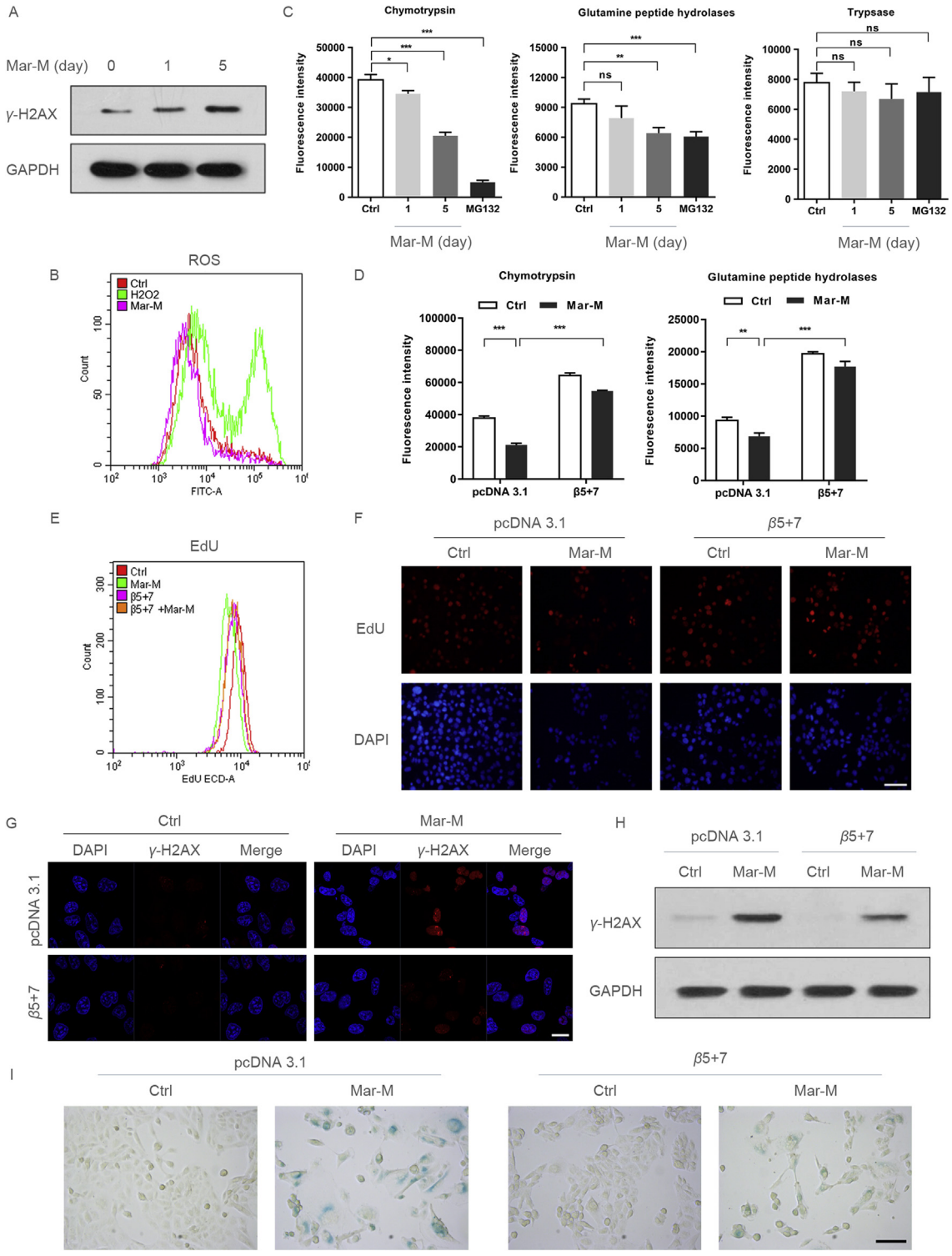

Figure 2 Mar-M-mediated proteasome inhibition is important for senescence induction. (A) Western blot analysis the expression of γ-H2AX in PC3/Doc cells treatment with Mar-M for 1 and 5 days. (B) Flow cytometry analysis the ROS in PC3/Doc cells treatment with Mar-M or H_2O_2 (12 h). (C) The analysis of proteasome activity in PC3/Doc cells treated with Mar-M for 1 and 5 days, MG132 was included as a positive control for 12 h. (D) The analysis of proteasome activity in PC3/Doc cells were transfected with β5 and β7, and treated with Mar-M. (E) Flow cytometry of EdU incorporation assay after transfected with β5 and β7, and treated with Mar-M. (F) Representative fluorescent images of EdU staining transfected with β5 and β7, and treated with Mar-M. Scale bar: 100 μm. (G) Confocal microscopic analysis of γ-H2AX in PC3/Doc cells treated with Mar-M after transfected with β5 and β7. Scale bar: 20 μm. (H) PC3/Doc cells transfected with β5 and β7 and treated with Mar-M for 5 days and Western blot analysis the expression of γ-H2AX. (I) Transfection of β5+β7 was performed in combination with Mar-M treatment and analysed the SA-β-gal activity. Scale bar: 100 μm. Results are representative of three independent experiments. Data are mean ± SD, $^{*}P < 0.05$, $^{**}P < 0.01$ and $^{***}P < 0.001$.

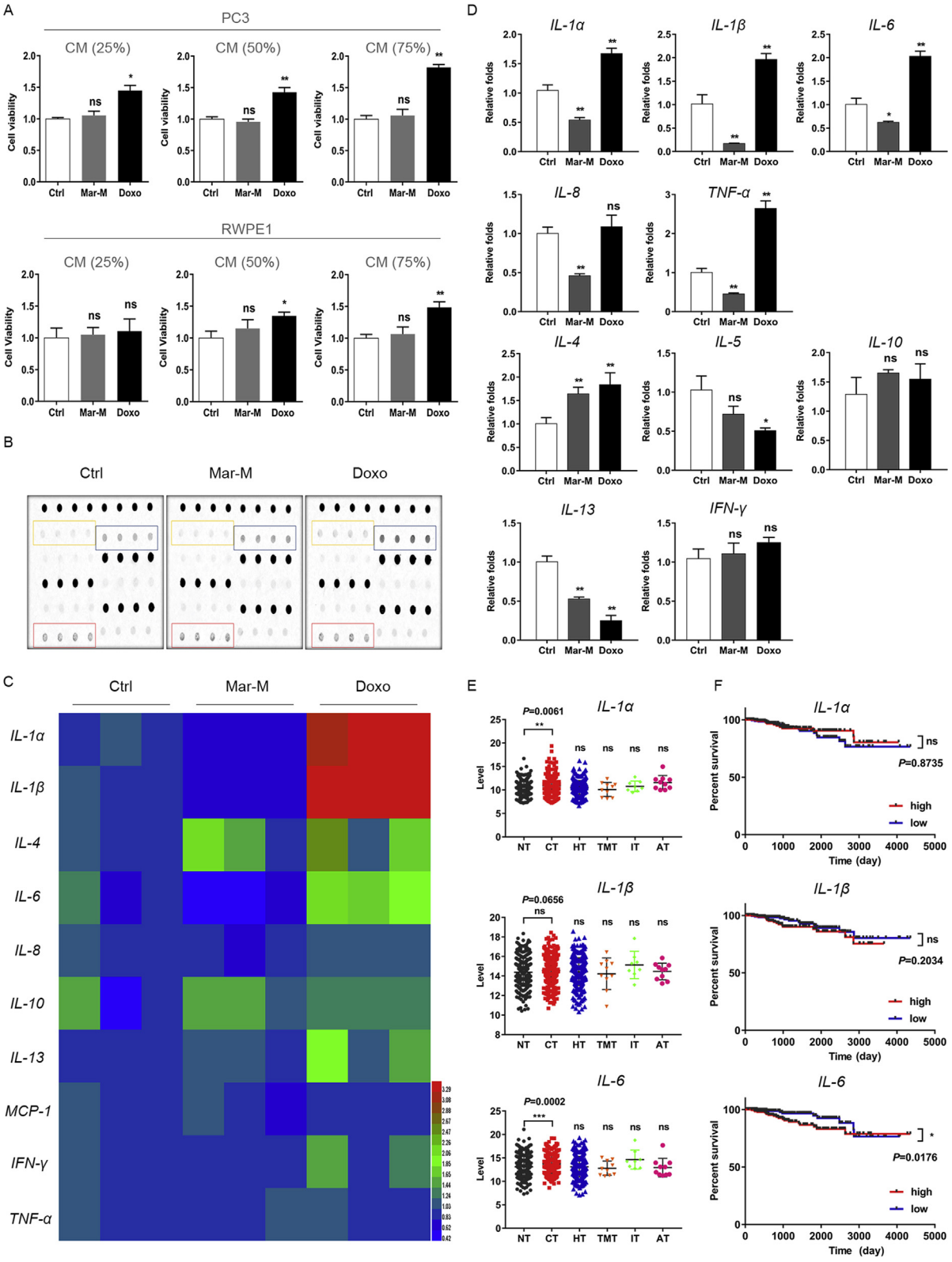

Figure 3 Mar-M suppress senescent cells expressing SASP. (A) Survival rate of PC3, RWPE1 treated with conditioned medium from senescent PC3/Doc cells. (B) Cytokine array blots for PC3/Doc cells that were treated with Mar-M or Doxo for 5 days. Cytokine levels of the supernatant were detected using cytokine array assay kit. (C) Cytokine levels of the supernatant were analyzed by heatmap. (D) The mRNA levels of cytokine and chemokine were detected with Q-PCR. Results are representative of three independent experiments. (E) Inflammation levels of different therapeutic method of breast carcinoma patients in TCGA. No therapy (NT), chemotherapy (CT), hormone therapy (HT), targeted molecular therapy (TMT), immunotherapy (IT), ancillary therapy (AT). (F) Overall survival plots of cytokine in TCGA patients that were treated with chemotherapy. Data are mean ± SD, $^{*}P < 0.05$, $^{**}P < 0.01$ and $^{***}P < 0.001$.

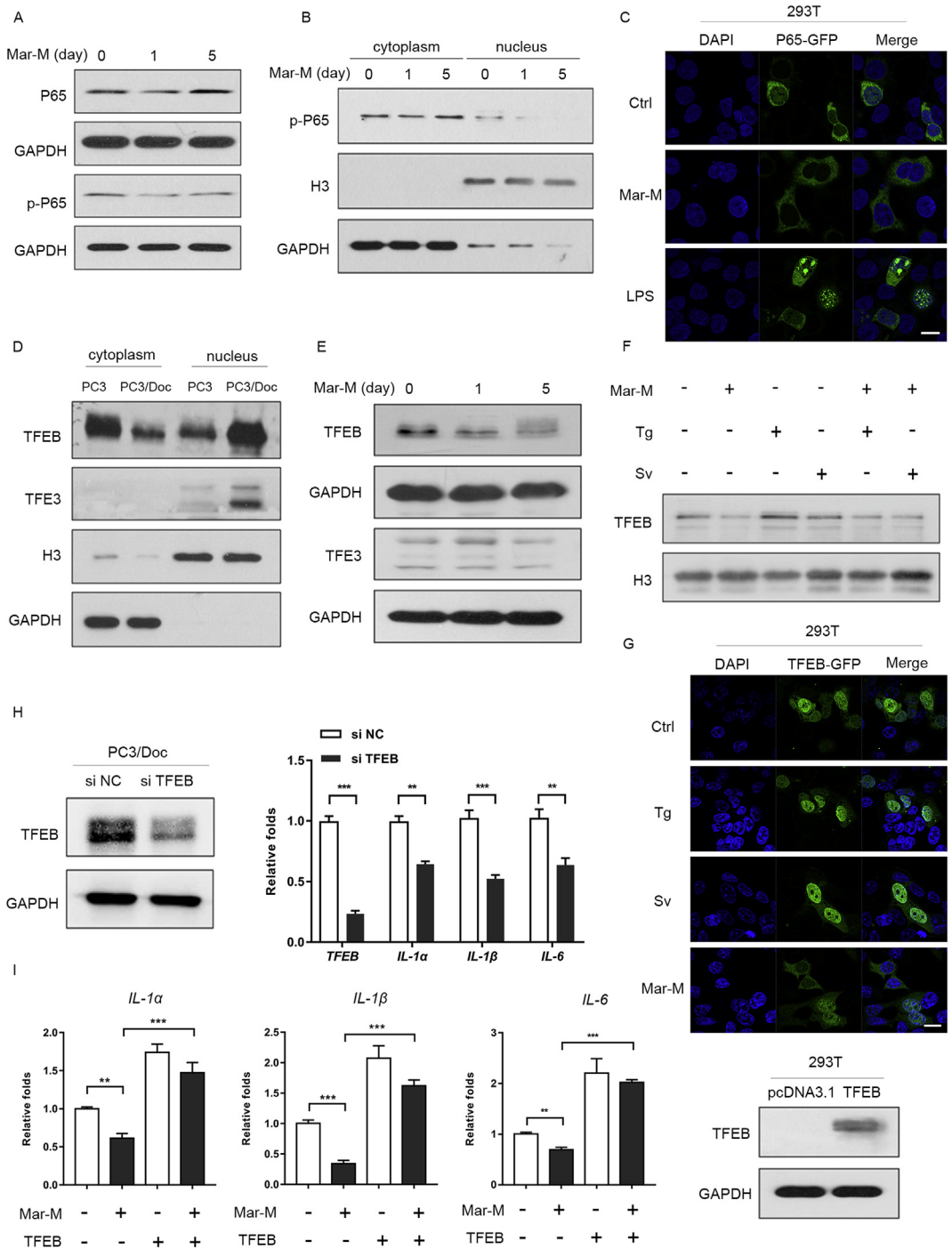

Figure 4 Inactivation of TFEB and NF-κB contributes to suppression of SASP by Mar-M. (A) Western blot analysis of the P65, the phspho-p65 (p-P65) in PC3/Doc cells treated with Mar-M. (B) Immunoblots of p-P65 state in nuclear and cytosolic fraction of PC3/Doc incubated with Mar-M for 1 or 5 days. GAPDH and Histone 3 (H3) were used as control. (C) The nuclear translocation of P65 was detected by confocal microscopy, LPS was used as positive control. (D) The nuclear and cytoplasmic fraction of TFEB and TFE3 in PC3/Doc cells and PC3 cells. (E) Western blot analysis of the TFEB and TFE3 in PC3/Doc cells treated with Mar-M. (F) Nuclear fraction of TFEB in PC3/Doc cells with Mar-M, thapsigargin (Tg) and Starvation (Sv). (G) Immunofluorescent staining of TFEB-GFP detected in 293T cells treated with Mar-M for 24 h and stained with DAPI (to visualize nuclei). Starvation and thapsigargin were used as positive controls for TFEB nuclear translation. (H) siRNA knockdown of TFEB in PC3/Doc cells was performed and analysed the *IL-1α*、*IL-1β* and *IL-6* levels. (I) Quantification of *IL-1α*、*IL-1β* and *IL-6* levels were shown after TFEB overexpression in 293T cell treated with Mar-M. Results are representative of three independent experiments. Data are mean ± SD, $^{*}P < 0.05$, $^{**}P < 0.01$ and $^{***}P < 0.001$. Scale bar: 20 μm.

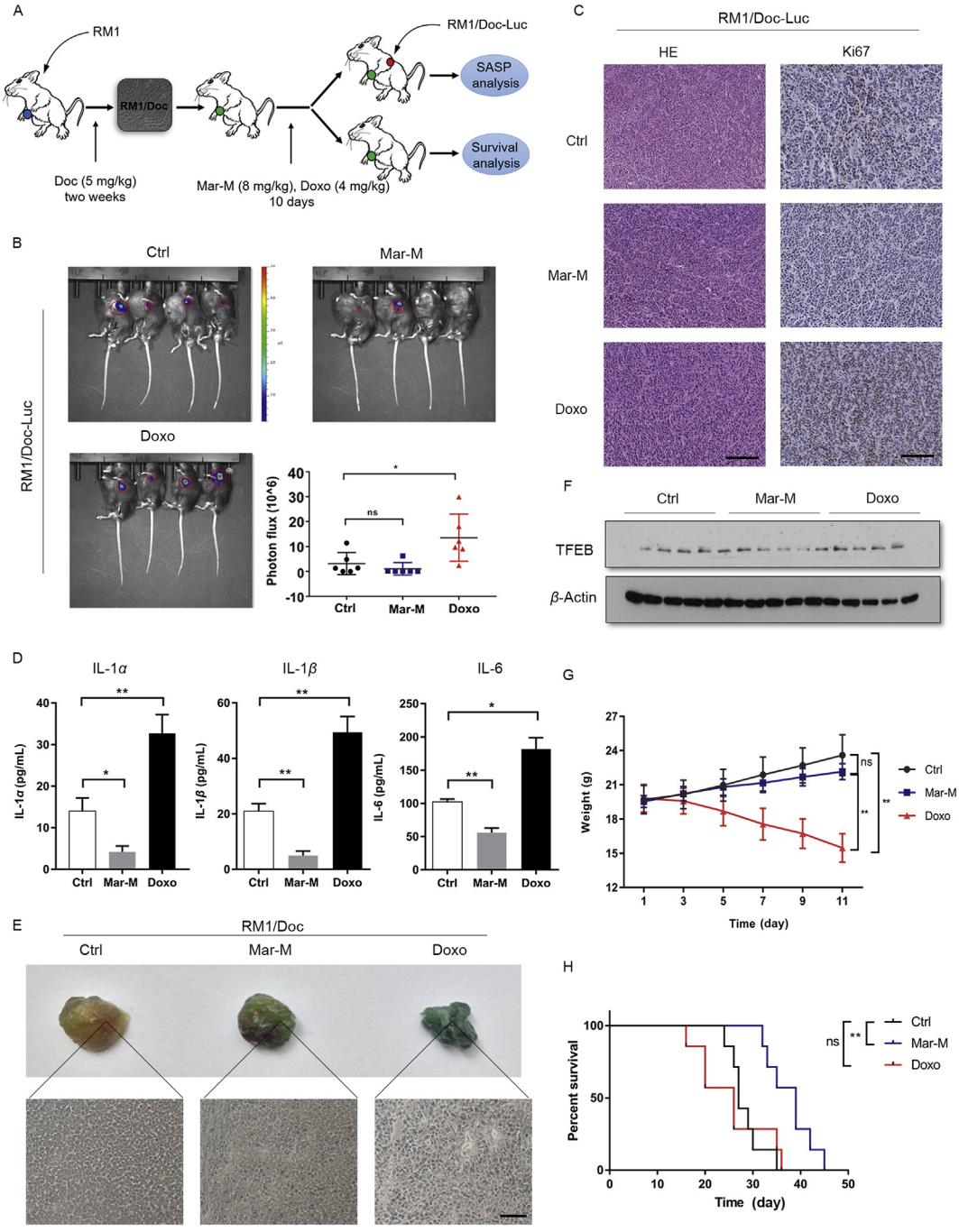

Figure 5 Mar-M exerts antitumor efficacy with prolonged survival and reduced paracrine of SASP in tumor-bearing homograft mice. (A) Animal model. The RM1 cells were injected into the mice and given docetaxel at 5 mg/kg allowed to establish RM1/Doc homograft. Tumor-bearing mice were randomly assigned to control and administration groups ($n = 13$). After 10-days treatment with either Mar-M or doxorubicin, the animals were randomly divided into two groups for different analysis. One group ($n = 6$) was designed to examine the paracrine effect of SASP, the other mice ($n = 7$) were maintained for survival analysis. (B) Tumors were quantified using bioluminescence imaging 10 days after injecting RM1/Doc-Luc cells. Statistical analysis of the tumor bioluminescene intensity is shown. (C) Positively stained cells for Ki67. (D) Levels of the proinflammatory cytokines IL-α, IL-1β, and IL-6 in C57 mice were measured using ELISA after treatment with Mar-M liposomes or Doxo. (E) Detection of SA-β-gal activity in control tissue, Mar-M tissue and Doxo tissue. Showing the absence of SA-β-gal positive cells in control tissue, whereas clearly positive cells can be observed in the Mar-M and Doxo groups. (F) Western blot analysis of the TFEB in tumor treated with Mar-M liposomes and Doxo. (G) Body weight of mice after treatment with Mar-M liposomes or Doxo. (H) RM1/Doc homograft mice model showed overall survival difference with Mar-M in comparison to control or Doxo. Data are mean ± SD, $^{*}P < 0.05$, $^{**}P < 0.01$ and $^{***}P < 0.001$. Scale bar: 100 μm.

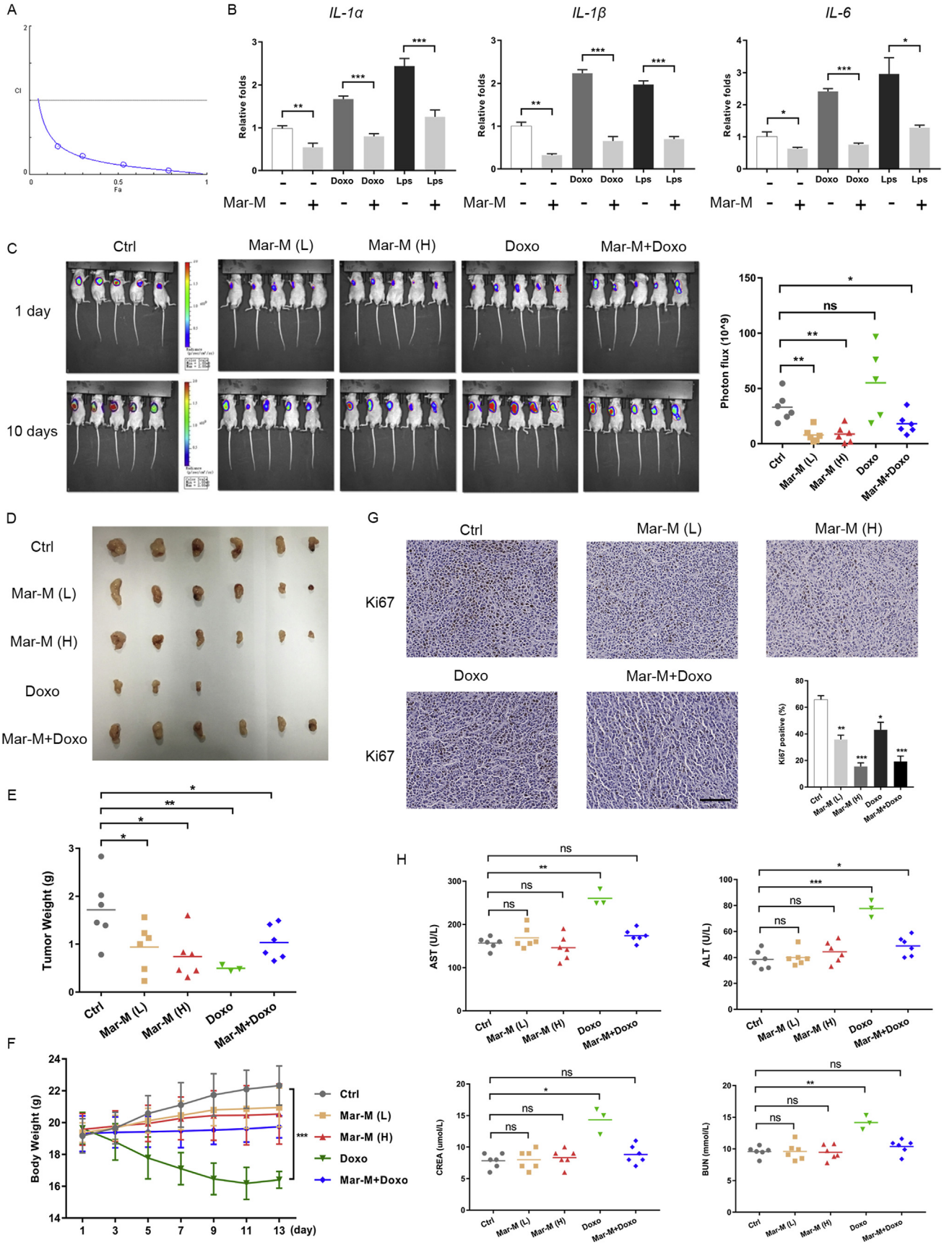
A
CI
Fa
B
IL-1α
IL-1β
IL-6
Relative folds
Mar-M
Doxo
Lps
C
Ctrl
Mar-M (L)
Mar-M (H)
Doxo
Mar-M+Doxo
1 day
10 days
Photon flux (10^9)
D
Ctrl
Mar-M (L)
Mar-M (H)
Doxo
Mar-M+Doxo
E
Tumor Weight (g)
F
Body Weight (g)
(day)
G
Ki67
Ki67 positive (%)
H
AST (U/L)
ALT (U/L)
CREA (umol/L)
BUN (mmol/L)
ns

stimulation of conditioned media (CM) from senescent PC3/Doc cells on PC3 and RWPE1 cells. As shown in Fig. 3A, a rapid increase in cell viability was noted when PC3 cells exposed to CM form Doxo-induced senescent cells with the increased CM in the fresh culture medium. However, CM from senescent cells treated with Mar-M had no stimulation in PC3 cells under the same experimental conditions (Fig. 3A). Similarly, CM from Mar-M-treated cells had limited effect on RWPE1 cell viability, while CM from cells exposed to Doxo exerted some promotion (Fig. 3A). These results indicated that Mar-M attenuated the potential of the secreted SASP on malignant promotion.

We therefore aimed to analyze the effect of Mar-M on major SASP components of senescent PC3/Doc cells using antibody arrays (Fig. 3B). As illustrated in Fig. 3C, Mar-M, to some extent, reduced the secretion of several pro-inflammatory proteins including *IL-1α*, *IL-1β*, *IL-6*, and *TNF-α*, associated with the decrease in *IL-8* and *IL-13*. However, Doxo treatment resulted in significant elevation in *IL-1α*, *IL-1β*, and *IL-6* in SASP. To verify the changes in SASP upon Mar-M treatment, we assessed the cytokine transcription by quantitative PCR assays. Consistent with the observations in Fig. 3C, Doxo significantly stimulated gene expression related to inflammation, however, the corresponding mRNA levels of *IL-1α*, *IL-1β*, *IL-6*, *IL-8*, *IL-13* and *TNF-α* were declined in response to Mar-M (Fig. 3D). Of note, *IL-10* and *INF-γ* remained unchanged in senescent cells following challenge with either Mar-M or Doxo, whereas elevated *IL-4* was observed in response to both chemicals (Fig. 3D).

In addition, analysis of changes in inflammatory cytokines (*IL-1α*, *IL-1β*, *IL-6*) of breast carcinoma patients upon different therapeutic methods (chemotherapy, hormone therapy, targeted molecular therapy, immunotherapy, ancillary therapy) in the Cancer Genome Atlas (TCGA), we noticed that, among of therapeutic options, chemotherapy (docetaxel or doxorubicin) was prone to inducing *IL-1α, IL-1β*, and *IL-6* (Fig. 3E). Moreover, reduced inflammation levels, such as *IL-6*, somehow are beneficial for overall survival (Fig. 3F). Taken together, Mar-M transcriptionally suppressed the inflammatory gene expressions, which in turn led to the reduced secretion of SASP.

3.4. *Mar-M-triggered inactivation of TFEB and NF-κB contributes to suppression of SASP*

Multiple factors have been found to regulate SASP, including transcription factors and some signal pathways[5,10]. It appears that most SASP regulators converge on the activation of transcription factor NF-κB and C/EBP, two transcriptional machineries that control the expression of diverse SASP components[20]. We therefore sought to examine whether Mar-M had an effect on the activation of NF-κB. Indeed, the phosphorylation of NF-κB subunit P65 (phosphor-P65) was reduced in senescent cells treated with Mar-M, while total P65 almost remained unaffected (Fig. 4A). Furthermore, less phosphor-P65 was detected in the nucleus in Mar-M-induced senescent cells (Fig. 4B), whereas abundant phosphor-P65 was evidenced in the cytoplasm due to constitutive activation of NF-κB in PC3 cells[21]. Immunofluorescence staining supported the observations that Mar-M suppressed the migration of P65 from cytoplasm to the nucleus (phosphor-P65), but LPS-induced P65 translocation, served as a positive control, was obvious (Fig. 4C)[22].

In addition to NF-κB, transcription factor TFEB and TFE3 have recently emerged as modulators for *IL-6* expression[23]. We were prompted to examine the involvement of TFEB and TFE3 in the regulation of SASP in senescent PC3/Doc cells, because activated TFEB and TFE3 (in the nucleus) was pronounced in PC3/Doc cells as compared to that of PC3 cells (Fig. 4D). The results indicated that a decreased TFEB, rather than TFE3, was noticeable in Mar-M-treated cells (Fig. 4E). To confirm the effect of Mar-M on the inactivation of TFEB, we examined the active form of TFEB in the nucleus. As shown in Fig. 4F, TFEB was markedly declined in the nucleus by Mar-M, while TFEB was enhanced upon thapsigargin (Tg) or starvation (Sv) which served as a positive control. In addition, Mar-M was able to suppress the activation of TFEB induced by Tg and Sv (Fig. 4F). Immunofluorescence analysis confirmed the reduction in TFEB nuclear translocation in Mar-M-induced senescent cells (Fig. 4G). To validate the importance of TFEB in regulation of inflammatory factors, the changes of SASP components were examined in cells overexpressing or knockdown of TFEB. As shown in Fig. 4H, knockdown TFEB alone could partly abolish the SASP in PC3/Doc cells. By contrast, ectopic expression of TFEB resulted in enhancement of *IL-1α*, *IL-1β*, and *IL-6*, leading to predominant restoration of SASP that were inhibited by Mar-M (Fig. 4I). Therefore, Mar-M suppressed the SASP components through inactivation of TFEB and NF-κB.

3.5. *Mar-M exerts antitumor efficacy with prolonged survival and inhibits the paracrine effect of SASP in tumor-bearing homograft mice*

We next evaluated whether Mar-M could alleviate tumor burden due to its ability in the induction of senescence and decrease of SASP using RM1/Doc-Luc homograft mice. Tumor-bearing RM1/Doc homograft mice were pretreated with Mar-M or Doxo for 10 days, the mice ($n = 6$) were subsequentially introduced RM1/Doc-luciferase (RM1/Doc-Luc) cells into the other side of each mouse to examine the paracrine effect of SASP released from RM1/Doc tumors. The paracrine effect of SASP was evaluated by measuring changes of bioluminescent luciferase in tumors arising from RM1/Doc-Luc. The fluorescence intensity of RM1/Doc-Luc tumors in mice that were pretreated with Mar-M was comparable to the control, while tumor

Figure 6 Mar-M is potently enhancing the antitumor efficacy of doxorubicin with little cytotoxicity in chemoresistant xenografts. (A) CI plot of synergism in Mar M and doxorubicin (CI value of less than 1 denotes synergism). (B) Real-time PCR was employed to analyzed mRNA levels of *IL-1α*、*IL-1β* and *IL-6* in cells exposed to chemicals (Mar-M, Doxo, LPS, Mar-M+Doxo and Mar-M+LPS). (C) Tumors were quantified using bioluminescence imaging treated with Placebo (Ctrl), Mar-M(L) (8 mg/kg), Mar-M(H) (16 mg/kg), Doxo (4 mg/kg) and Mar-M plus Doxo (4 mg/kg+2 mg/kg). Significant changes in bioluminescence intensity (Photon flux; photon/s/cm^2/square root between control and experimental mice). (D) Photographs of excised tumors from five groups are shown. (E) Weights of tumors from five groups are shown. (F) Body weight from mice in different groups was recorded every 2 days. (G) Ki67 stains of tumors tissues. Ki67-positive rates in each group. Scatter plot shows the % of positively stained nuclei. (H) Biochemical analysis of liver and renal function. Data are mean ± SD, $^{*}P < 0.05$, $^{**}P < 0.01$ and $^{***}P < 0.001$. Scale bar: 100 μm.

growth was noticeably accelerated in Doxo-pretreated mice (Fig. 5B), indicating that SASP released from RM1/Doc tumors, which were pretreated with Mar-M, had little paracrine effect on RM1/Doc-Luc tumor growth. Also, positively stained Ki67 cells in RM1/Doc-Luc tumors were significantly declined with Mar-M treatment, but increased Ki67 positive cells were present in tumors treated with Doxo (Fig. 5C). Analysis of typical markers of SASP verified that Mar-M markedly inhibited the expressions of IL-1α, IL-1β, and IL-6, whereas Doxo significantly stimulated the expression of these factors (Fig. 5D), in agreement with the observations in cultured cells (Fig. 3). We then moved to examine the effect of Mar-M on senescence induction in RM1/Doc tumor samples. Indeed, Mar-M induced RM1/Doc tumor senescent as evidenced by increased SA-β-gal staining (Fig. 5E), consistent with results in cultured cells. It appeared that Doxo exerted more potential ability on cellular senescence induction (Fig. 5E). Also, it was noted that TFEB was reduced in Mar-M-treated tissue samples, but not in samples treated with Doxo (Fig. 5F). These results indicated that limited change in RM1/Doc-Luc tumor growth might be owing to the suppressive effect of Mar-M on SASP. Thus, transcriptional down-regulation of the SASP components during senescence induction by Mar-M resulted in alleviated the deleterious paracrine effect of SASP in promoting tumor growth. We next observed that Mar-M had no significant effect on body weight in tumor-bearing mice compared to the placebo control, while Doxo significantly reduced the body weight of mice (Fig. 5G). At the same time, Mar-M significantly increased mice survival, which was much longer than the placebo or mice treated with Doxo (Fig. 5H). Survival over 40 days with treatment in mouse xenografts generally predicts for high response and survival in human clinical trails[24]. Taken together, Mar-M exerted antitumor efficacy on chemoresistant mice through induction of cancer cellular senescence, which associated with prolonged survival and suppressed the SASP in promoting tumor progression.

3.6. Mar-M synergistically cooperates with doxorubicin, resulting in enhanced antitumor efficacy with little cytotoxicity in chemoresistant xenografts

Considering the contribution of pro-inflammatory cytokines and SASP to chemoresistance[25], together with the effect of Mar-M on pro-inflammatory components of SASP, we further validated the antitumor efficiency and toxicity of Mar-M and investigated whether Mar-M might also be effective in alleviating the proinflammatory response of Doxo on human chemoresistant PC3/Doc xenografts. The results in Fig. 6A demonstrated that Mar-M and Doxo displayed extremely low combinatory index (CI) value (CI value of less than 1 denotes synergism)[26], indicating their significant synergism to inhibit resistant cell proliferation. Analysis of the alterations in inflammatory cytokines revealed that Mar-M effectively reversed the expressions of *IL-1α*, *IL-1β*, and *IL-6*, which were upregulated by either LPS or Doxo (Fig. 6B).

We next investigated the potential antitumor efficacy of this drug combination in PC3/Doc xenografts. Cohort groups were composed of mice randomly assigned to receive placebo, single agents (Mar-M or Doxo), or the combination therapy (Mar-M plus Doxo). One mouse died at day-10 and two animals failed to complete the study in the Doxo group due to its toxicity. Endpoint analyses displayed that, whether delivered individually or in combination, Mar-M(L) (8 mg/kg), Mar-M(H) (16 mg/kg) and Mar-M plus Doxo (4 mg/kg+2 mg/kg) were effectively against tumor growth potential as evidenced by much weaker fluorescence intensity in treated-mice than that of the control (Fig. 6C). The tumor weights were highest in the control (1.72 $\pm$ 0.69 g), decreased to 0.99 $\pm$ 0.53 and 0.74 $\pm$ 0.47 g in mice treated with Mar-M(L) and Mar-M(H), respectively (Fig. 6D and E). Doxo exerted a strong inhibition as indicated by the lowest tumor weight (0.50 $\pm$ 0.06 g) among of these treatments (Fig. 6D and E). Of noted, the tumor, somehow, remained growth ability in mice treated with Doxo (Fig. 6C), although Doxo potently killed cancer cells (Fig. 6D and E). Combination therapy with Mar-M at 4 mg/kg plus Doxo at 2 mg/kg also pronouncedly inhibited tumor growth (1.03 $\pm$ 0.36 g) (Fig. 6D and E), but with much less toxicity, owing to a loss of body weight in Doxo-treated mice significantly recovered in the presence of Mar-M (Fig. 6F). Remarkably, the body weights remained almost unchanged in mice receiving Mar-M alone, no matter at 8 mg/kg or 16 mg/kg, respectively (Fig. 6F). Also, in the presence of Mar-M, a loss of body weight in Doxo-treated mice was significantly recovered as shown in Fig. 6F. Proliferation index verified the inhibition of Mar-M in tumor growth, a decrease in the Ki67 positivity 35.7 $\pm$ 1.6%, 15.5 $\pm$ 1.3%, 43 $\pm$ 2.8% and 19.2 $\pm$ 2.0% was observed in tumor samples treated by Mar-M(L), Mar-M(H), Doxo and Mar-M plus Doxo, respectively, compared to the control mice (65.7 $\pm$ 1.6%) as shown in Fig. 6G. Furthermore, Mar-M had no detectable effect on mouse liver and renal function, because no significant changes in aspartate transaminase (AST), glutamic-pyruvic transaminase (ALT), blood urea nitrogen (BUN), and creatinine (CREA) were observed in tissue samples from the treated mice (Fig. 6H). Combination treatment clearly attenuated the increase of AST, ALT, BUN and CREA, which had been markedly stimulated by Doxo (Fig. 6H). Therefore, Mar-M exerted antitumor efficacy in chemoresistant mice with limited toxicity, and acted synergistically with Doxo to inhibit tumor growth.

4. Discussion

In this study, we discovered novel actions of bisbibenzyls as inhibitors of the proliferation of chemoresistant PCa by promoting senescence and suppressing the secretion of SASP. First, Mar-M, acting as an anti-inflammatory bisbibenzyl, induces senescence of chemoresistant cancer cells largely independent of P53 at low concentrations, making it possible to use low doses of this agent to overcome the obstacle and achieve successful treatment. Second, Mar-M significantly suppresses the expression of the components of SASP, and substantially reduces the stimulation effects of the SASP on either cultured cells, or nearby tumor growth *in vivo*. Third, normal fibroblasts are much more resistant to Mar-M, without detectable toxicity in homograft and xenograft-bearing mice. Combination of Mar-M ameliorates the toxicity of Doxo, achieving a greater efficacy in mice, which indicates that Mar-M would be a promising drug due to its selectivity and low toxicity. Further, our data indicate that, in addition to NF-κB, TFEB is also important in the regulation of SASP components during senescence induction by Mar-M.

Although the SASP is beneficial for tissue repair, wound healing, and immune surveillance, increasing lines of evidence suggest that the SASP can also be deleterious and is responsible for the onset of age-related diseases, particularly cancer

resistance, relapse and metastasis[9,25]. For example, senescent cells accumulate after genotoxic anticancer therapeutics, and the secretion of SASP may cause or contribute to the drug resistance and cancer recurrence that frequently follow such therapies[27]. One strategy has proposed specific blockade of SASP components by targeting their upstream regulators and effectors[25]. Several transcription factors and signaling pathways and extensive crosstalk among them are involved in controlling diverse SASP factors at the transcription level, or protein level, including NF-κB and C/EBP-β, as well as PI3K−AKT−mTOR, p38MAPK, TGF-β, cGAS−STING[10].

Targeting these individual critical molecules can result in substantial attenuation or abrogation of the SASP. To this end, many efforts have been made to discover various agents, including small-molecule compounds and antibodies, to effectively block the SASP. For example, given the regulatory effects of mTOR on SASP, mTOR inhibitors, such as rapamycin and its analogs, were selected to suppress the SASP by reducing the expression of membrane-bound IL-1α, which provides a potential basis for developing small molecules to reduce the detrimental consequences of genotoxic therapies[28]. Metformin, a clinically approved drug for diabetes, blocks NF-κB translocation to the nucleus, thereby reducing its transcriptional activity on SASP[29]. Therefore, current efforts are largely invested in the discovery of active agents targeting the SASP and clearing senescent cells.

Our study identified Mar-M as a novel naturally occurring bisbibenzyl to induce drug-resistant cancer cellular senescence with little toxicity, and has no influence on the proliferation of non-neoplastic cells (RWPE1) and normal human fibroblast cells (NHF). Importantly, our findings indicate that Mar-M might suppress chemotherapy-driven cancer progression by its down-regulatory effect on SASP development. It is well documented that numerous inflammatory factors are regulated by NF-κB signaling pathway, particularly, the IL-6 and IL-1α, can form positive feedback loops with NF-κB during senescence[30]. In addition to NF-κB that was inactivated by Mar-M, our data demonstrated that the decrease in TFEB nuclear localization also contributed to the reduced inflammatory factors in Mar-M-mediated senescence induction. TFEB is a recently identified transcription factor that controls lysosomal biogenesis and autophagy[31]. We found that TFEB and TFE3 were significantly activated in PCa cells after treatment with docetaxel. However, the enhancement of TFEB in resistant cells was blocked upon Mar-M treatment *via* the alteration of its nucleus translocation. We also examined the regulatory effect of several clinically used agents, such as docetaxel, Doxo on TFEB and TFE3. It appears that all drugs exert either stimulation or have limited impact on TFEB (data not shown), except Mar-M that inhibits TFEB activation, implicating a unique intervention of Mar-M on TFEB. How Mar-M regulates TFEB, as well as NF-κB, requires further investigation.

In summary, our findings identify suppression of the SASP components as a novel mechanism by which bisbibenzyl Mar-M induces cancer cellular senescence with little toxicity, and might prevent cancer relapse. Understanding how the SASP is controlled by Mar-M could provide an approach to overcome chemoresistance.

Acknowledgments

This work was supported by the National Natural Science Foundation of China (81473238, 81872896, and 81874293), and the Shandong Key Innovative Research Program (2018CXGC1216, China).

Appendix A. Supporting information

Supporting data to this article can be found online at https://doi.org/10.1016/j.apsb.2019.08.007.

References

1. Ewald J, Desotelle J, Almassi N, Jarrard D. Drug-induced senescence bystander proliferation in prostate cancer cells *in vitro* and *in vivo*. *Br J Canc* 2008;**98**:1244−9.
2. Sha M, Mao G, Wang G, Chen Y, Wu X, Wang Z. DZNep inhibits the proliferation of colon cancer HCT116 cells by inducing senescence and apoptosis. *Acta Pharm Sin B* 2015;**5**:188−93.
3. He S, Sharpless NE. Senescence in health and disease. *Cell* 2017;**169**:1000−11.
4. Herranz N, Gil J. Mechanisms and functions of cellular senescence. *J Clin Investig* 2018;**128**:1238−46.
5. Tchkonia T, Zhu Y, van Deursen J, Campisi J, Kirkland JL. Cellular senescence and the senescent secretory phenotype: therapeutic opportunities. *J Clin Investig* 2013;**123**:966−72.
6. Velarde MC, Demaria M, Campisi J. Senescent cells and their secretory phenotype as targets for cancer therapy. *Interdiscip Top Gerontol* 2013;**38**:17−27.
7. Sagiv A, Krizhanovsky V. Immunosurveillance of senescent cells: the bright side of the senescence program. *Biogerontology* 2013;**14**:617−28.
8. Hernandez-Segura A, Nehme J, Demaria M. Hallmarks of cellular senescence. *Trends Cell Biol* 2018;**28**:436−53.
9. Ovadya Y, Krizhanovsky V. Strategies targeting cellular senescence. *J Clin Investig* 2018;**128**:1247−54.
10. Sun Y, Coppe JP, Lam EW. Cellular senescence: the sought or the unwanted?. *Trends Mol Med* 2018;**24**:871−85.
11. Maria J, Ingrid Z. Effects of bioactive compounds on senescence and components of senescence associated secretory phenotypes *in vitro*. *Food Funct* 2017;**8**:2394−418.
12. Malavolta M, Costarelli L, Giacconi R, Piacenza F, Basso A, Pierpaoli E, et al. Modulators of cellular senescence: mechanisms, promises, and challenges from *in vitro* studies with dietary bioactive compounds. *Nutr Res* 2014;**34**:1017−35.
13. Han DW, Lee MH, Kim B, Lee JJ, Hyon SH, Park JC. Preventive effects of epigallocatechin-3-*O*-gallate against replicative senescence associated with p53 acetylation in human dermal fibroblasts. *Oxid Med Cell Longev* 2012;**2012**:850684.
14. Lim H, Park H, Kim HP. Effects of flavonoids on senescence-associated secretory phenotype formation from bleomycin-induced senescence in BJ fibroblasts. *Biochem Pharmacol* 2015;**96**:337−48.
15. Zhang N, Li Z, Xu K, Wang Y, Wang Z. Resveratrol protects against high-fat diet induced renal pathological damage and cell senescence by activating SIRT1. *Biol Pharm Bull* 2016;**39**:1448−54.
16. Luo H, Yang A, Schulte BA, Wargovich MJ, Wang GY. Resveratrol induces premature senescence in lung cancer cells *via* ROS-mediated DNA damage. *PLoS One* 2013;**8**:e60065.
17. Jiang H, Sun J, Xu Q, Liu Y, Wei J, Young CY, et al. Marchantin M: a novel inhibitor of proteasome induces autophagic cell death in prostate cancer cells. *Cell Death Dis* 2013;**4**:e761.

18. Niu L, Deng J, Zhu F, Zhou N, Tian K, Yuan H, et al. Anti-inflammatory effect of marchantin M contributes to sensitization of prostate cancer cells to docetaxel. *Cancer Lett* 2014;**348**:126−34.
19. Zhang D, Cui Y, Niu L, Xu X, Tian K, Young CY, et al. Regulation of SOD2 and beta-arrestin 1 by interleukin-6 contributes to the increase of IGF-1R expression in docetaxel resistant prostate cancer cells. *Eur J Cell Biol* 2014;**93**:289−98.
20. Malaquin N, Martinez A, Rodier F. Keeping the senescence secretome under control: molecular reins on the senescence-associated secretory phenotype. *Exp Gerontol* 2016;**82**:39−49.
21. O'Neill AJ, Prencipe M, Dowling C, Fan Y, Mulrane L, Gallagher WM, et al. Characterisation and manipulation of docetaxel resistant prostate cancer cell lines. *Mol Cancer* 2011;**10**:126.
22. Siegert I, Schodel J, Nairz M, Schatz V, Dettmer K, Dick C, et al. Ferritin-mediated iron sequestration stabilizes hypoxia-inducible factor-1 alpha upon LPS activation in the presence of ample oxygen. *Cell Rep* 2015;**13**:2048−55.
23. Pastore N, Brady OA, Diab HI, Martina JA, Sun L, Huynh T, et al. TFEB and TFE3 cooperate in the regulation of the innate immune response in activated macrophages. *Autophagy* 2016;**12**:1240−58.
24. Talmadge JE, Singh RK, Fidler IJ, Raz A. Murine models to evaluate novel and conventional therapeutic strategies for cancer. *Am J Pathol* 2007;**170**:793−804.
25. Zhang B, Lam EW, Sun Y. Senescent cells: a new Achilles' heel to exploit for cancer medicine?. *Aging Cell* 2019;**18**:e12875.
26. Chou TC. Theoretical basis, experimental design, and computerized simulation of synergism and antagonism in drug combination studies. *Pharmacol Rev* 2006;**58**:621−81.
27. Sun Y, Campisi J, Higano C, Beer TM, Porter P, Coleman I, et al. Treatment-induced damage to the tumor microenvironment promotes prostate cancer therapy resistance through WNT16B. *Nat Med* 2012;**18**:1359−68.
28. Laberge RM, Sun Y, Orjalo AV, Patil CK, Freund A, Zhou L, et al. MTOR regulates the pro-tumorigenic senescence-associated secretory phenotype by promoting IL1A translation. *Nat Cell Biol* 2015;**17**:1049−61.
29. Moiseeva O, Deschenes-Simard X, St-Germain E, Igelmann S, Huot G, Cadar AE, et al. Metformin inhibits the senescence-associated secretory phenotype by interfering with IKK/NF-kappaB activation. *Aging Cell* 2013;**12**:489−98.
30. Crescenzi E, Pacifico F, Lavorgna A, De Palma R, D'Aiuto E, Palumbo G, et al. NF-kappaB-dependent cytokine secretion controls Fas expression on chemotherapy-induced premature senescent tumor cells. *Oncogene* 2011;**30**:2707−17.
31. Brady OA, Martina JA, Puertollano R. Emerging roles for TFEB in the immune response and inflammation. *Autophagy* 2018;**14**:181−9.